JPE 19-1-5

https://doi.org/10.6113/JPE.2019.19.1.44
ISSN(Print): 1598-2092 / ISSN(Online): 2093-4718

Design of LLCL Filter for Single Phase Inverters with Confined Band Variable Switching Frequency (CB-VSF) PWM

Hussain A. Attia†, Tan Kheng Suan Freddy**, Hang Seng Che*, and Ahmad H. El Khateb***

†,*UM Power Energy Dedicated Advanced Centre, University of Malaya, Kuala Lumpur, Malaysia
**Faculty of Computing, Engineering and Technology, Asia Pacific University, Kuala Lumpur, Malaysia
***School of Electronics, Electrical Engineering and Computer Science, Queen's University Belfast, Belfast, NI, UK

Abstract

Recently, the use of LLCL filters for grid inverters has been suggested to give better harmonic attenuation than the commonly used L and LCL filters, particularly around the switching frequency. Nevertheless, this filter is mainly designed for constant switching frequency pulse width modulation (CSF PWM) methods. In variable switching frequency PWM (VSF PWM), the harmonic components are distributed across a wide frequency band which complicates the use of a high order filter, including LCL and LLCL filters. Recently, a confined band variable switching frequency (CB-VSF) PWM method has been proposed and demonstrated to be superior to the conventional constant switching frequency (CSF) PWM in terms of switching losses. However, the applicability of LLCL filters for this type of CB-VSF PWM has not been discussed. In this paper, the authors study the suitability of an LLCL filter for CB-VSF PWM and propose design guidelines for the filter parameters. Using simulation and experimental results, it is demonstrated that the effectiveness of an LLCL filter with CB-VSF PWM depends on the parameters of the filters as well as the designed variable frequency band of the PWM. Simulation results confirm the performance of the suggested LLCL design, which is further validated using a lab scale prototype.

Key words: Confined band variable switching frequency CB-VSF PWM, Constant switching frequency PWM (CSF PWM), LCL filter, LLCL filter

NOMENCLATURE

L_1	Inverter side inductor
L_2	Grid side inductor
C_f	Filter capacitor (tuning branch)
X_{Cf}	Capacitive impedance of C_f
C_{fmin}	Minimum value of the filter capacitor
C_{fmin}	Maximum value of the filter capacitor
L_f	Filter inductor (tuning branch)
X_{Lf}	Inductive impedance of L_f
Z_{LfCf}	Impedance of the tuning branch (L_fC_f)
$G(s)$	TRANSFER FUNCTION
$I_{inv}(s)$	Inverter side current
$V_{inv}(s)$	Inverter side voltage
f_s	Switching frequency
f_{tune}	Tuned frequency
nf_s	Multiples of the switching frequency
f_r	Resonance switching frequency
f_g	Grid frequency
f_{VSF}	Variable switching frequency
$f_{CB\text{-}VSF}$	Confined band variable switching frequency
f_{VSFmin}	Minimum variable switching frequency
ω, ω_g	Grid angular frequency.
ω_r	Resonant angular frequency.
ω_{tune}	Tuned angular frequency
ω_s	Switching angular frequency
ω_{VSF}	Variable switching angular frequency
ω_{VSFmin}	Minimum variable switching angular frequency
k	Constant value equal to ($L_1 \cdot L_2/L_1+L_2$)

Manuscript received Jun. 5, 2018; accepted Oct. 25, 2018
Recommended for publication by Associate Editor Joung-Hu Park.
†Corresponding Author: hussainaa6969@yahoo.com
Tel: +603-22463246, UMPEDAC, University of Malaya
*UM Power Energy Dedicated Adv. Centre, Univ. Malaya, Malaysia
**Faculty of Computing, Eng. Technol., Asia Pacific Univ., Malaysia
***Sch. Electron., Electr. Eng. Comput. Sci., Queen's Univ. Belfast, UK

α	Square value of the rate of f_r to f_{tune}
V_g	Grid voltage
P_{rated}	System rated power
I_{ref}	Peak value of the system rated current
V_{dc}	DC link voltage
B	Constant parameter in CB-VSF PWM

I. INTRODUCTION

In the application of direct current (DC) renewable energy sources, such as PVs, an inverter is necessary to convert DC power to AC power for grid integration. To have higher performance grid connected systems, stringent requirements on the power quality of inverters have been introduced. For example, according to IEC-1000–3 [1] and/or IEEE Standard 519-1992 [2], the total harmonic distortion (THD) of the output current generated by an inverter should be limited to below 5%.

In order to comply with grid requirements, low pass filters are employed to attenuate high frequency harmonics [3]-[9]. Single inductor filters, i.e. L filters [3], [4], provide a simple and low cost first order filtering function. However, they are bulky and not very effective. Consequently, higher order low pass filters, such as LCL [3], [5]-[9] (Fig. 1(a)) and LLCL [6], [10]-[13] (Fig. 1 (b)) filters have been proposed in order to meet grid interconnection standards with reduced size and cost as well as better higher order harmonics attenuation when compared to L filters.

In order to overcome resonance, various damping methods have been proposed in the literature [14], [15]. Various types of passive damping methods were studied and investigated in [15]. A generalized model of the LCL filter with various passive damping configurations and corresponding transfer functions were developed. Based on the model and transfer function, the LCL filters were designed to meet design criteria. Active damping for LCL filters was proposed in [14]. The active damping was achieved via a virtual resistor without any additional sensors when compared to conventional damping methods.

With an additional resonant branch (L_f and C_f), as shown in Fig. 1(b), the LLCL filter is effective in eliminating the switching frequency harmonic components, which leads to an improved THD when compared to the LCL filter. Although comprehensive design procedures for LCL and LLCL filters have been proposed and evaluated, they are designated for constant switching frequency pulse width modulation (CSF PWM) applications, and cannot be directly applied to variable switching frequency PWM (VSF PWM). When compared to CSF PWM, VSF PWM has the advantages of lower audible noise [16] and lower switching losses [17]. However, the harmonic components in VSF PWM are distributed across a wide frequency band, which complicates the filter design. Recently, the authors of [18] demonstrated that by using confined band VSF PWM (CB-VSF PWM), the switching harmonics components are confined within a predetermined band and can be safely used with an LLCL filter without exciting its resonance frequency. Since the dominant harmonics in CBVSF-PWM are still around the switching frequency, the use of an LLCL filter can be advantageous in further suppressing the switching harmonics, while maintaining a small filter size. However, previous discussions on the selection of LLCL filter parameters have been specific for CSF PWM based inverters. It is unclear how the design guideline will be different for CBVSF-PWM since the harmonics spectra is different from that of the CSF PWM.

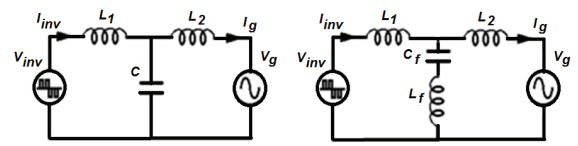

(a) (b)

Fig. 1. Equivalent circuit diagram of: (a) LCL Filter; (b) LLCL Filter.

In this study, the authors investigate the parameter selections for an LLCL filter when applied with the CBVSF-PWM method.

Unlike the CSF-PWM case, an LLCL-filter for CBVSF-PWM should be designed to have a broader attenuation along the band to suppress harmonics above the switching frequency within the variable switching frequency band, instead of just ensuring good attenuation which is obtained at the switching frequency. The effects of the L and C values on the performance of an LLCL filter are validated via simulation and experimental results.

This paper is organized as follows. In Section II, a comparison of the current harmonic spectrums between CSF PWM and CB-VSF PWM schemes is presented. Then the characteristics of LCL and LLCL filters as well as the effects of filter transfer functions on harmonic attenuation are investigated. Section III discusses the design considerations of an LLCL filter for a CB-VSF PWM single phase inverter. Meanwhile, the LLCL filter parameters implementation is described in Section IV. Section V presents simulation results in addition to an analysis of the filter performance. In Section VI, the theoretical analysis and simulation results are validated via a 1 kW inverter prototype. Guidelines for the LLCL filter component design steps are presented for CB-VSF PWM in Section VII. Finally, a summary of the findings is given in Section VIII.

II. PWM HARMONIC SPECTRUM AND FILTER RESPONSES

A. CSF- PWM Harmonic Spectrum

For carrier based PWM where the carrier signal has a fixed frequency, the PWM is considered to be constant switching frequency PWM (CSF-PWM). The harmonic spectrum of

CSF PWM [6] is well known as shown in Fig. 2(a), with switching harmonics appearing around nf_s, where f_s is the switching frequency and n = {1, 2, 3 …}. In terms of magnitude, the harmonics around n =1 have the highest magnitude and are quickly reduced as n increases.

B. CB-VSF PWM Harmonic Spectrum

The CB-VSF PWM scheme is proposed in [18] such that the switching frequency is varied within a predefined frequency band. The variable switching frequency range of CB-VSF PWM is confined between minimum and maximum switching frequencies with the highest amplitude at the minimum switching frequency f_{VSFmin} as presented in Fig. 2(b). The confined frequency band ensures that CB-VSF PWM does not create harmonics that coincide with the resonance frequency of the filter.

C. Harmonic Spectrum Similarities and Differences Between CSF PWM and CB-VSF PWM

For both of the PWM schemes, the highest harmonic component appears approximately around multiples of the effective switching frequency, whereas the dominant harmonics appear at the first effective switching frequency. On the other hand, the distributions of harmonic components are quite different. The harmonic components for CSF PWM concentrate around multiples of the switching frequency, while harmonics for CB-VSF PWM spread out over a frequency band depending on the design of the CB-VSF PWM [18]. Nevertheless, the highest harmonic component of CB-VSF PWM is always lower than that of CSF PWM as shown in Fig. 2(a) and Fig. 2(b), which were obtained at the same parameters and serial filter value (5 mH) for the two PWM schemes. Since the harmonic spectra of CBVSF-PWM is different from that of CSF-PWM, the filter must be designed so that the harmonic components in the frequency band are effectively attenuated.

D. LLCL Filter Response

Passive power filters are commonly used in full-bridge inverters as shown in Fig. 3. The transfer functions of the LLCL filter can be derived as [6], [10]:

$$G_{V_{inv}\to I_{inv}}(s) = \frac{I_{inv}(s)}{V_{inv}(s)}\Big|_{V_g(s)=0} = \frac{(L_2+L_f)\,C_f\,s^2+1}{(L_1\,L_2\,C_f+(L_1+L_2)\,L_f\,C_f)\,s^3+(L_1+L_2)\,s} \quad (1)$$

$$G_{V_{inv}\to I_g}(s) = \frac{I_g(s)}{V_{inv}(s)}\Big|_{V_g(s)=0} = \frac{L_f\,C_f\,s^2+1}{(L_1\,L_2\,C_f+(L_1+L_2)\,L_f\,C_f)\,s^3+(L_1+L_2)\,s} \quad (2)$$

$$f_r = \frac{1}{2\pi\sqrt{\left(\frac{L_1L_2}{L_1+L_2}+L_f\right)C_f}} \quad (3)$$

$$f_{tune} = \frac{1}{2\pi\sqrt{L_fC_f}} \quad (4)$$

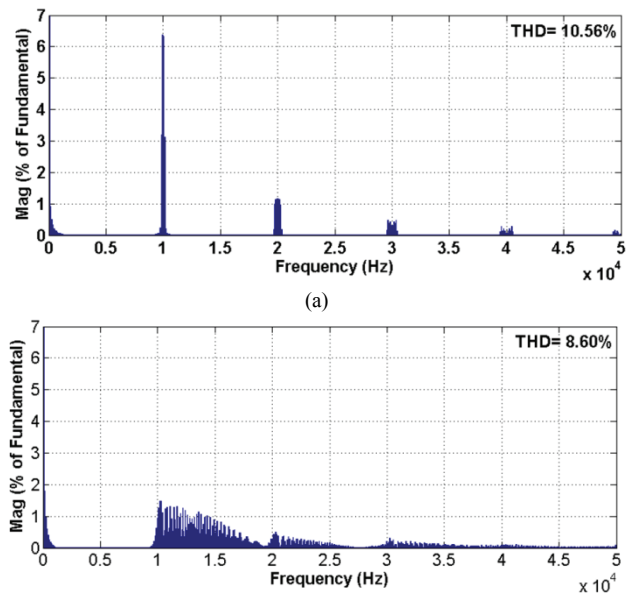

(b)

Fig. 2. Harmonic current spectrum of an inverter through a serial 5 mH filter: (a) With CSF PWM of f_S = 10 kHz; (b) With CB-VSF PWM, f_{VSF} = 10 kHz-20 kHz.

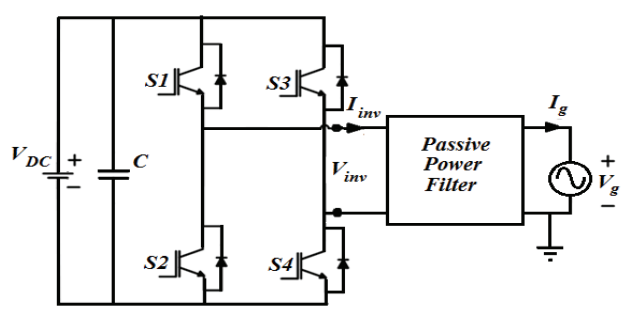

Fig. 3. Single-phase full-bridge inverter with a passive power filter.

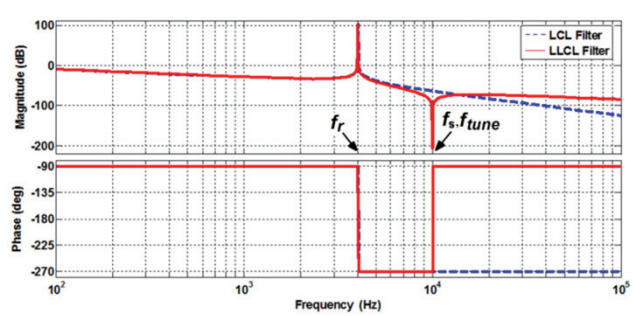

Fig. 4. Bode plots of LCL and LLCL filters for the transfer function of $I_g(s)/V_{inv}(s)$.

The resonance frequency f_r represents the frequency at which the harmonics are amplified as shown in Fig. 4. This must be avoided in the design of the PWM and the filter. The use of a "confined band" in CBVSF-PWM ensures that this can be achieved easily for VSF-PWM. On the other hand, the harmonics that appear at f_{tune} are significantly attenuated. It is worth highlighting that the LLCL filter provides better

attenuation than the LCL filter for frequencies around f_{tune}. However, this advantage diminishes for frequencies further above f_{tune}.

For CSF-PWM, the design is focused on selecting f_{tune} to be equal to the effective switching frequency, and adjusting the rest of the parameters to minimize L and C, while maintaining the losses and THD. Since CBVSF-PWM has different harmonics spectra, it is necessary to reexamine the design guidelines, with the following points taken into consideration:

i) Knowing that the highest harmonic component is still around the effective switching frequency, f_{tune} should be selected around this frequency.
ii) The resonance frequency should be higher than 10 times the fundamental frequency (grid frequency) f_g but lower than half the effective switching frequency [6].
iii) The output current ripple and reactive power from the capacitor should be within acceptable ranges.
iv) The L and C values should be selected to maximize the attenuation effect while satisfying conditions (i) – (iii).

In this study, a fixed serial inductance (L_1 + L_2) is considered to limit the voltage drop of these inductors and to focus on analyzing the effect of C_f & L_f variations on the attenuation effectiveness of the LLCL filter.

III. LLCL Filter Design Considerations for CB-VSF PWM Based Single Phase Inverters

In this section, an analysis is done by looking at the design requirement for each of the components in an LLCL filter.

A. Inverter Side Inductor L_1

The value of the inverter side filter inductor (L_1) should agree with the constrain of the maximum ripple of the switching frequency on the inverter side current, which is commonly accepted to be in the range of 15% to 40% as shown in (5) [6]:

$$15\% \leq \frac{V_{dc}}{4\ L_1 f_s I_{ref}} \leq 40\% \tag{5}$$

Where V_{dc} is the DC link voltage, f_s is the switching frequency, and I_{ref} is the peak value of the rated current.

This parameter will be considered as a fixed value in subsequent discussions.

B. Allowable Component Ranges of the L_f &C_f Tuning Branch

Similar to the case of CSF PWM, the maximum allowable limit of absorbed reactive power should be restricted to 5% of the rated system power [6]. This gives the maximum limit of C_f as (6):

$$C_{fmax} = \frac{5\%\ P_{rated}}{V_g^2\ \omega_g} \tag{6}$$

Where P_{rated} is the system rated power, V_g is the root mean square value of the grid voltage, ω_g is $2\pi f_g$, and f_g is the grid frequency.

To ensure the suppression of the dominant switching harmonics, the values of $L_f C_f$ should be chosen so that the tuning frequency is equal to the effective switching frequency, i.e.:

$$\frac{1}{L_f C_f} = {\omega_{VSFmin}}^2 = {\omega_s}^2 = {\omega_{tune}}^2 \tag{7}$$

However, the choice of C_f affects the resonance frequency, as dictated by (3). This means that while satisfying the maximum condition at (6), the high filter capacitor negatively effects the stability of the grid current [10], and the acceptable values of C_f should take the allowable range of the resonance frequency into consideration (10 $f_g < f_r < 0.5\ f_s$), such that:

$$10\omega_g < \frac{1}{\sqrt{\left(\frac{L_1 L_2}{L_1+L_2} + L_f\right)C_f}} < 0.5\omega_s \tag{8}$$

The value of L_1 is determined by (5) and L_f is evaluated from (7). Based on (8), it is clear that L_2 and C_f are two factors that need to be optimized together. The selection of L_2 is discussed subsequently.

Reducing C_f degrades the attenuation effectiveness, the minimum allowable value of C_f is limited by the maximum allowable value of the resonance frequency f_r, which is equal to half of the switching frequency. Therefore, the case of C_f (0.5 μF) is selected to explain the effect of exceeding the minimum limit of C_f.

The minimum allowable C_f can be determined for each of the L_1 and L_2 values by starting from the resonance frequency f_r relationship shown in (9) [13] for the LLCL filter components:

$$(2\pi f_r)^2 = \frac{1}{\left(\frac{L_1 L_2}{L_1+L_2} + L_f\right)C_f} \tag{9}$$

At fixed L_1 and L_2 values, the minimum value of the filter capacitor can be obtained by considering the maximum allowable value of the resonance frequency $f_r = 0.5\ f_s$. Hence, the resonance relationship of (9) can be written as follows:

$$(2\pi * 0.5 f_s)^2 = \frac{1}{(k + L_f)C_f} \tag{10}$$

Where the constant k is $\frac{L_1 L_2}{L_1+L_2}$.

From (7), L_f can be written as function of C_f:

$$L_f = \frac{1}{4\pi^2 f_s^2\ C_f} \tag{11}$$

Substituting (11) into (10) yields (12):

$$C_f = \frac{1}{\pi^2 f_s^2\ k + \frac{1}{4C_f}} = \frac{4C_f}{4\pi^2 f_s^2\ k\ C_f + 1} \tag{12}$$

The value of C_f in (12) represents the minimum value of

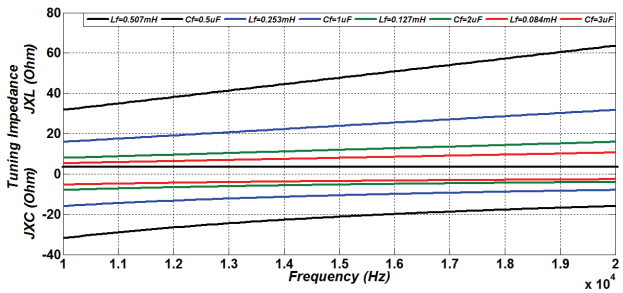

(a)

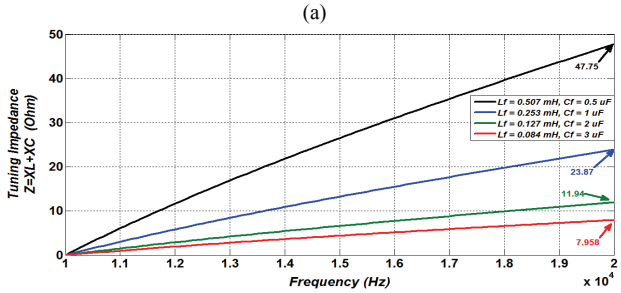

(b)

Fig. 5. Four inductive and capacitive impedances variations with respect to the range of the frequency: (a) *XL* and *XC* impedances; (b) Equivalent impedance.

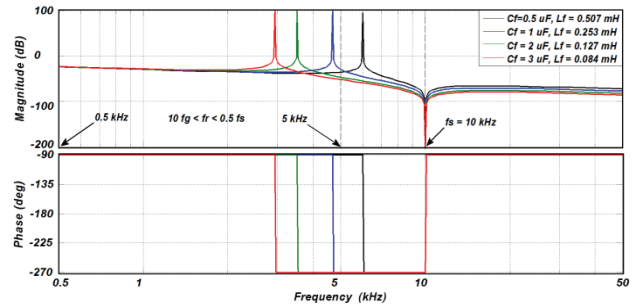

(a)

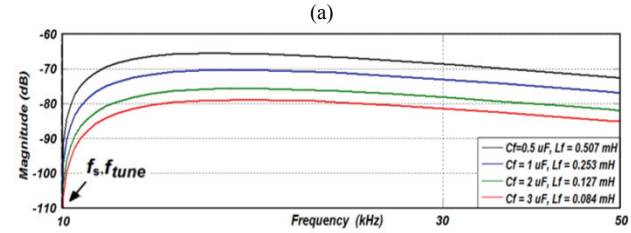

(b)

Fig. 6. LLCL Bode plots at fixed values of L_1 & L_2 and at different values of C_f & L_f of the same tuning: (a) Allowable resonance frequency f_r range; (b) Zoom in for the switching frequency location and above.

the filter capacitor C_{fmin} because it is derived at the condition of the maximum resonance frequency f_r. The minimum value of C_{fmin} can be found from (13) after re-arranging (12):

$$C_{fmin} = \frac{3}{4\pi^2 f_s^2 \ k} \tag{13}$$

There are multiple combinations of C_f and L_f values that can satisfy conditions (6), (7) and (13). To understand the effect of changing C_f on the LLCL filter response, four values 0.5 μF, 1 μF, 2 μF and 3 μF are selected for demonstration purposes. By keeping f_{tune} at 10 kHz, the corresponding calculated L_f values are 0.507 mH, 0.253 mH, 0.127 mH and 0.084 mH, respectively. The ability to attenuate harmonics using the C_fL_f branch is determined by the value of the equivalent impedance of $Z_{LfCf} = X_{Lf} + X_{Cf}$. Since a lower impedance Z_{LfCf} gives better attenuation, the combination of L_f=0.084 mH and C_f =3 μF is expected to be better than the case with L_f= 0.507 mH and C_f =0.5 μF.

Variations of X_L and X_C for the selected L_f and C_f values are shown in Fig. 5. From Fig. 5(b), it can be observed that the differences among the impedance magnitudes reduce with the value of C_f rising. It can also be noticed that the impedance of L_f (0.084 mH) and C_f (3 μF) at 20 kHz is equal to 7.958 Ω, which is markedly less than the impedance 47.75 Ω of L_f (0.507 mH) and C_f (0.5 μF). At the same time, the difference of 11.94 Ω - 7.958 Ω is equal to 3.982 Ω, which is less than the difference of 47.75 Ω – 23.87, which is equal to 23.88 Ω.

Fig. 6 shows four Bode plots of an LLCL filter at four different C_f and L_f values of the same tuning (10 kHz), whereas the inverter side inductor L_1 and the grid side inductor L_2 are fixed. Fig. 6 shows the effect of changing C_f and L_f on the LLCL filter attenuation above the switching frequency.

From Fig. 6, it can be seen that increasing C_f reduces the resonance frequency f_r and vice versa. Furthermore, increasing the C_f value increases the attenuation of harmonics above f_r. In particular, the attenuation for frequencies above f_s, i.e. where the switching harmonics of the CBVSF-PWM are located, increases with a higher C_f. Nevertheless, the improvement in attenuation is reduced with an increasing C_f. For example, from the zoomed in graph of Fig. 6(b), increasing C_f from 1 μF to 2 μF improves the attenuation by -5.5 *dB*. However, increasing C_f from 2 μF to 3 μF only improves the attenuation by -3.5 *dB*. It is clear that even though C_f should be maximized to improve harmonics attenuation. However, increasing C_f too much results in the absorbed reactive power increasing with a marginal gain in attenuation.

As a tradeoff between attenuation and losses, it is proposed here that the value of C_f is selected by averaging its maximum and minimum limits as shown in (14):

$$C_f = \frac{C_{fmax} + C_{fmin}}{2} \tag{14}$$

C. Allowable Range of the Grid Side Inductance L_2

In order to determine the values of C_f based on (14), it is necessary to decide the value of L_2. For CSF PWM, L_2 is selected to ensure that the harmonic components at the effective switching frequency are lower than 0.3% [6] in accordance with IEEE519-1992. For VSF PWM, the harmonic components are always lower than those of CSF PWM. Hence, the same (14) used in [6] for L_2 selection in CSF PWM is sufficient to ensure compliance with IEEE519-1992.

In addition, the choice of L_2 should take into consideration

the effect of the resonance frequency as in (8). L_2 can be expressed as a function of the resonance frequency as follows:

$$L_2 = \frac{(1-\omega_r^2 L_f C_f)\, L_1}{\omega_r^2 L_1 C_f + \omega_r^2 L_f C_f - 1} \tag{15}$$

Substituting (7) into (15) yields (16):

$$L_2 = \frac{\left[1-\left(\frac{\omega_r}{\omega_{tune}}\right)^2\right] L_1}{\left(\frac{\omega_r}{\omega_{tune}}\right)^2 \frac{L_1}{L_f} + \left(\frac{\omega_r}{\omega_{tune}}\right)^2 - 1} \tag{16}$$

Assume:

$$\left(\frac{\omega_r}{\omega_{tune}}\right)^2 = \alpha \tag{17}$$

Substituting (17) into (16) yields (18):

$$L_2 = \frac{(1-\alpha)\, L_1}{\left(1+\frac{L_1}{L_f}\right)\alpha - 1} \tag{18}$$

From (18), the value of L_2 can be expressed in terms of C_f:

$$L_2 = \frac{(1-\alpha)\, L_1}{(1+\omega_{tune}^2 L_1 C_f)\, \alpha - 1} \tag{19}$$

Since, the values of L_1 and ω_{tune} can be directly selected, the value of α is bounded by the resonance frequency limits $10 f_g < f_r < 0.5 f_s$, while the maximum value of C_f is bounded by (6). In addition, the feasible values of L_2 can be calculated for different combinations of C_f and α. By crosschecking the obtained L_2 values with the IEEE519-1992 harmonic requirement [6], final values of L_2 and C_f can be decided.

IV. Implementation of LLCL Filter Design Consideration for a CB-VSF PWM Based Single Phase Inverter

To conceptualize the design procedure discussed above, an example of its implementation is discussed here. A single-phase inverter with a CB-VSF PWM and an LLCL filter is considered here with the parameters given in Table I.

Based on the system parameters shown in Table I, the calculated L_1 is 3.55 mH and the selected value is 3.6 mH. For the minimum variable switching frequency f_{VSFmin} of 10 kHz with a fixed L_1 of 3.6 mH, the reasonable range of α for 0.5 kHz < f_r < 5 kHz, is 0.0025 < α < 0.25. Based on (17), the range of the allowable L_2 value can be determined using (18) or (19) for each of the tuned values of C_f and L_f. Using the Table I parameters, the maximum value of the tuning branch capacitor C_{fmax} = 3.09 μF is obtained using (6). Hence, the allowable values of L_2 can be calculated for 0.0025 < α < 0.25 and 0.5 μF < C_f < 3.0 μF as shown in Fig. 7. As demonstrated in Fig. 6(b), the required value of L_2 is reduced with an increase in C_f as well as an increase in α.

To guarantee that the attenuations for each of the harmonic components around and above the double switching frequency are equal to or less than 0.3%, the attenuation of harmonics order >35 can be calculated using the method in [6] for different combinations of L_2, C_f and L_f, as shown in Fig. 8.

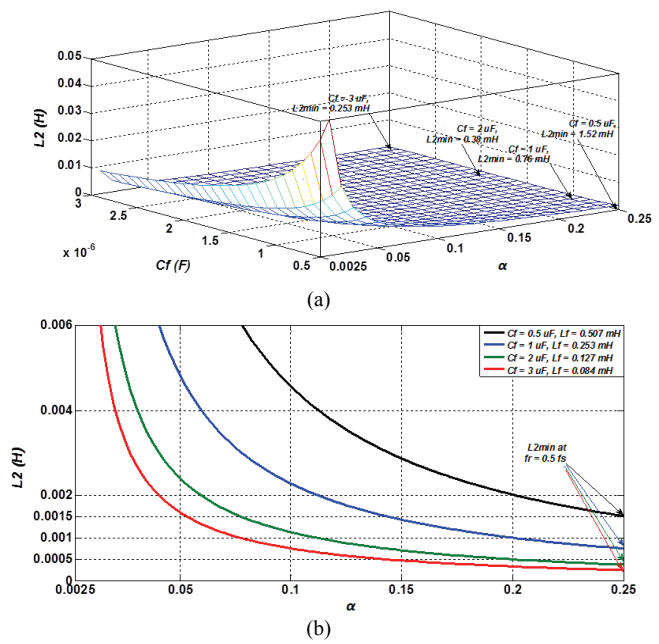

Fig. 7. Different ranges of L_2 along the allowable range of α for each C_f value: (a) 3D variation graph; (b) 2D variation graph.

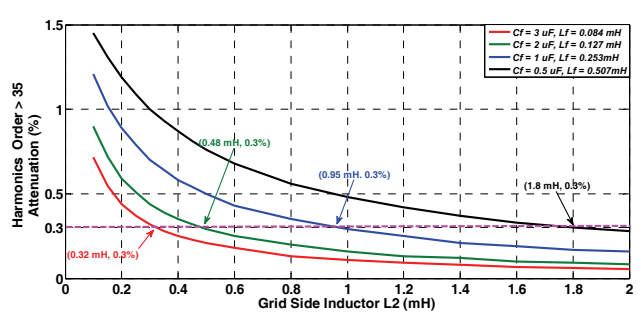

Fig. 8. Minimum limit of L_2 for an LLCL filter based on [6].

Note that L_f and C_f maintain the same tuning frequency at 10 kHz. From Fig. 8, as the value of C_f increases, the value of L_2 needs to be reduced. Based on the plots in Fig. 7 and Fig. 8, the lower the values of L_2 in the allowable ranges are inversely proportional to C_f. In other words, the lower L_2 is equal to 0.3 mH when C_f is equal to 3 μF, and it is 1.5 mH when C_f is equal to 0.5 μF. The selected value of L_2 is 1.2 mH to avoid the necessity of selecting the highest C_f value. The L_2 value is fixed in this study to focus on the effect of L_f and C_f variations on the LLCL filter attenuation along the different bands of CB-VSF PWM.

With selected values of L_1 (3.6 mH) and L_2 (1.2 mH), the calculated minimum capacitor is C_{fmin} = 0.844 μF. According to (14), the suitable designed value of C_f is 1.967 μF. Therefore, C_f = 2 μF is selected. Cross-checking with Fig. 8, it is clear that the selected value of 1.2 mH is well above the minimum 0.48 mH required to meet grid harmonics requirements.

In order to confirm the validity of the proposed LLCL filter design guidelines, simulation and experimental studies have

TABLE I
INVERTER SPECIFICATIONS

Parameters	Value
Input dc link voltage, V_{DC}	350 V
Rated power	1 kW
f_{VSFmax} for different band of CB-VSF PWM and R-VSF PWM	5 kHz
Adopted Strategy	Unipolar PWM
Dead time, T_d	2 µs
DC-link capacitors	2200 µF, 400 V
IGBT with ultrafast soft recovery diode	IRG4PH50KDPbF [21] V_{CES} = 1200V, I_C = 24A
Load resistor	50 Ω
Modulation Index, m	0.85
Current Ripple Factor, ΔI_{ref}	40% of I_{ref}

TABLE II
SIMULATED AND EXPERIMENTAL FILTER COMPONENTS (10 KHZ TUNING)

Component	LLCL Filter:1	LLCL Filter:2	LLCL Filter:3	LLCL Filter:4
L_1	3.6 mH	3.6 mH	3.6 mH	3.6 mH
L_2	1.2 mH	1.2 mH	1.2 mH	1.2 mH
C_f	0.5 µF	1 µF	2 µF	3 µF
L_f	507 µH	253 µH	127 µH	84 µH

been conducted. Different variable switching frequency bands were investigated through a unipolar PWM strategy [20] for a single-phase inverter. Table II shows the LLCL filter components with four different combinations of L_f and C_f. The first three cases use L and C values within the allowable ranges presented in the guidelines. Meanwhile, in the fourth case, C_f (0.5 µF) was selected to be lower than the minimum limit of C_f. This is to show the effect of a low capacitance on the production of high impedance Z_{LfCf}, which consequently leads to high THD levels in the load current spectrum.

V. SIMULATION RESULTS

MATLAB/Simulink is adopted to simulate a single-phase full-bridge inverter with an LLCL filter. Simulations results are recorded based on the parameters listed in Table I and Table II. The LLCL filter performance is investigated using four different values of L_f with four different C_f under the condition of the same tuning (10 kHz).

The filter performance is evaluated in terms of the harmonic reduction effectiveness starting from 10 kHz and the zero-switching-band total harmonic distortion (THD) i.e. CSF PWM. Then the filter performance is evaluated at different frequency bands. Analyses and comparisons are carried out for a 5 kHz CSF PWM along with 5-6 kHz, 5-7.5 kHz, 5-10 kHz and 5-15 kHz CB-VSF PWM based on the unipolar PWM strategy, which leads to harmonics appearing at twice the above mentioned switching frequencies. In other words, the effective switching frequency for CSF PWM is 10 kHz. Meanwhile, for CB-VSF PWM, the switching frequency bands are (10-12 kHz), (10-15 kHz), (10-20 kHz) and (10-30 kHz) respectively.

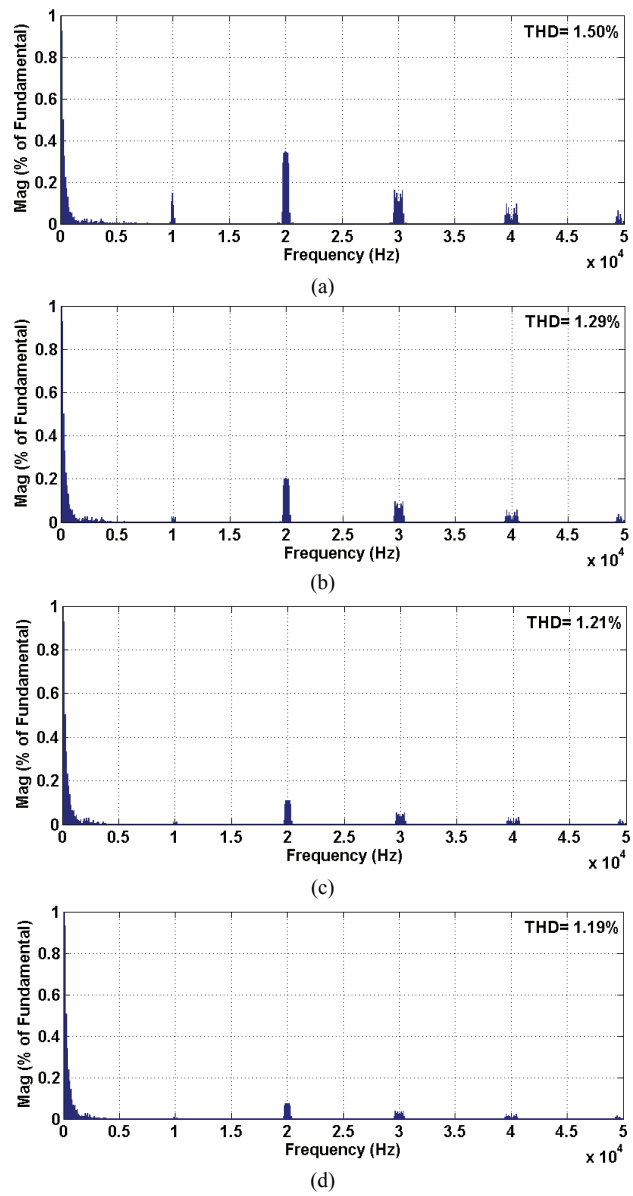

Fig. 9. Simulated harmonic spectrums of the load current based on 10 kHz CSF PWM using LLCL filters of the same tuning at f_s: (a) C_f = 0.5 µF, L_f = 0.507 mH; (b) C_f = 1 µF, L_f = 0.253 mH; (c) C_f = 2 µF, L_f = 0.127 mH; (d) C_f = 3 µF, L_f = 0.084 mH.

Fig. 9 shows the harmonic spectrums of load currents for 10 kHz PWM using four LLCL filters. It is clear that the LLCL filter is able to provide good attenuation around the tuning frequency. However, it is slightly less effective in suppressing higher frequency harmonics. In addition, C_f increasing has a positive effect on the overall harmonic suppression capability of the LLCL filter. However, even the current THD improves with C_f increasing this improvement become marginal as C_f continues to increase, which agrees with previous theoretical discussion.

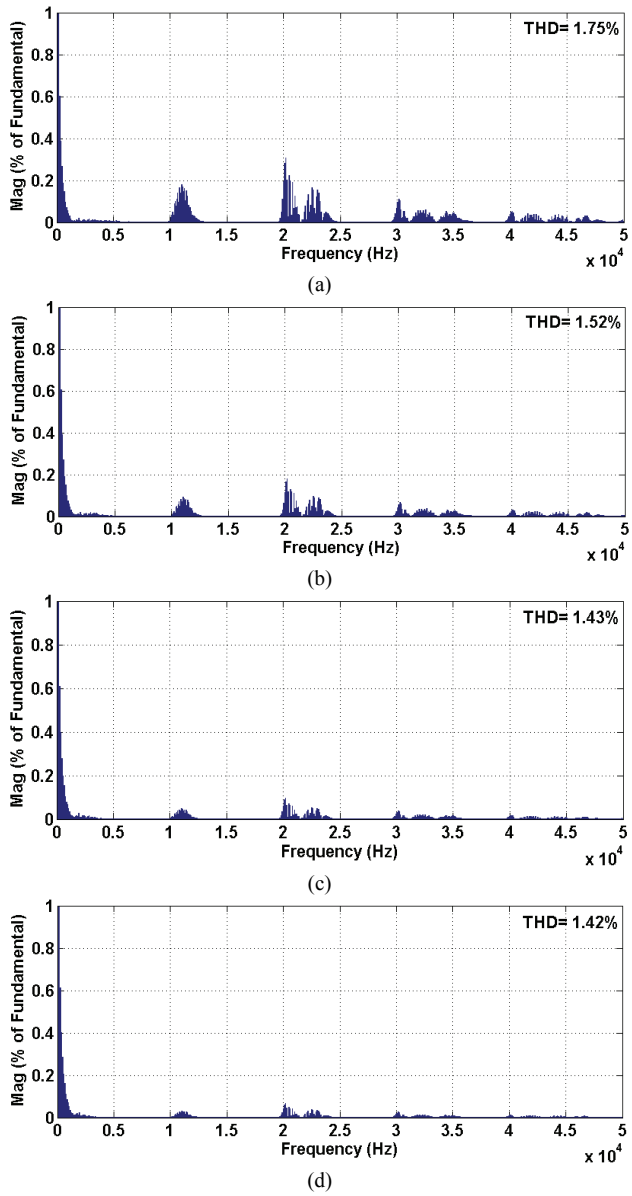

Fig. 10. Simulated harmonic spectrums of load current based on 10-12 kHz CB-VSF PWM using LLCL filters of the same tuning at f_{VSFmin}: (a) C_f = 0.5 μF, L_f = 0.507 mH; (b) C_f = 1 μF, L_f = 0.253 mH; (c) C_f = 2 μF, L_f = 0.127 mH; (d) C_f = 3 μF, L_f = 0.084 mH.

Fig. 10 shows the effect of four LLCL filters on the harmonic spectrums of the load currents for CB-VSF PWM with a small band, i.e. 10-12 kHz (2 kHz band). Similar to CSF PWM, C_f increasing improves the current THD, but with marginal enhancements for further C_f increases.

The LLCL filter behavior for CB-VSF PWM with a wider band of 10-30 kHz (20 kHz band) is shown in Fig. 11 via the reflected harmonic spectrums of the load currents. For the same LLCL filter, the THDs in Fig. 11 are higher than those in Fig. 10. This is due to the fact that as the CBVSF band increases, the switching harmonics begin spreading out above the switching frequency. Since the attenuation capability of the LLCL filter is mainly around the switching frequency, it becomes less effective as the harmonic spectrum spreads out over a wider frequency range. A higher C_f value is needed to obtain a better THD. To illustrate the performance of the LLCL filter under different VSF bands and filter parameters, simulations were carried out for different VSF bands with the results being summarized in Table III and illustrated in Fig. 12.

TABLE III
SIMULATED THD LEVELS OF LOAD CURRENTS USING FOUR FILTERS OF SAME TUNING AT 10 KHZ FOR DIFFERENT SWITCHING FREQUENCY BANDS

Switching Frequency	LLCL: 1 L_f=0.507 mH C_f=0.5μF	LLCL: 2 L_f=0.253 mH C_f= 1μF	LLCL:3 L_f=0.127 mH C_f= 2μF	LLCL:4 L_f= 0.084 mH C_f= 3 μF
CSF PWM f_s=10 kHz	1.5	1.29	1.21	1.19
CB-VSF PWM f_{VSF}=10-12 kHz	1.75	1.52	1.43	1.42
CB-VSF PWM f_{VSF}=10-15 kHz	2.16	1.86	1.76	1.74
CB-VSF PWM f_{VSF}=10-20 kHz	2.69	2.38	2.28	2.27
CB-VSF PWM f_{VSF} = 10-30 kHz	3.61	3.38	3.31	3.30

It is clear that the harmonic suppression capability of the LLCL filter is reduced with increases of the VSF band, due to the fact that the LLCL filter is better at attenuating harmonics around the tuning frequency. As discussed earlier, increasing C_f improves the overall harmonic suppression capability, and the enhancement becomes marginal with further increases in C_f. Fig. 13 shows the THD enhancement based on (20) with respect to the filter capacitor range; (0.5-1 μF), (1-2 μF), and (2-3 μF). From Fig. 13, it is noticeable that there is enhancement in the THD percentage levels for all of the filter capacitor ranges. Meanwhile, the enhancement percentage is small for the filter capacitor (2-3 μF).

Therefore, there is no need to select the highest value of the filter capacitor to simultaneously avoid absorbing the maximum part of the system reactive power and avoid the negative effect on system stability [10].

In addition, the THD level enhancement is small at the wide 20 kHz band due to higher harmonic spectrums along the high frequency locations starting from f_{VSFmin} (10 kHz).

$$THD\ Enhcement\ \% = \frac{|THD_1\% - THD_2\%|}{THD_1\%} * 100\% \qquad (20)$$

The simulation results in Section 5 confirmed the theoretical

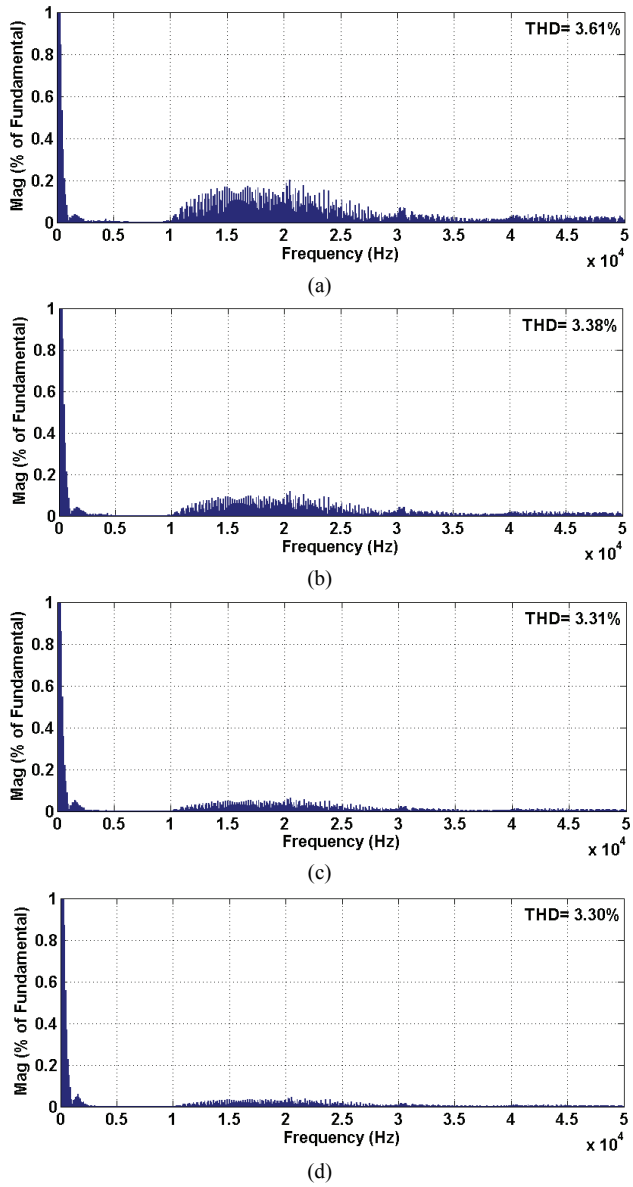

Fig. 11. Simulated harmonic spectrums of load current based on 10-30 kHz CB-VSF PWM using LLCL filters of the same tuning at f_{VSFmin}: (a) C_f = 0.5 μF, L_f = 0.507 mH; (b) C_f = 1 μF, L_f = 0.253 mH; (c) C_f = 2 μF, L_f = 0.127 mH; (d) C_f = 3 μF, L_f = 0.084 mH.

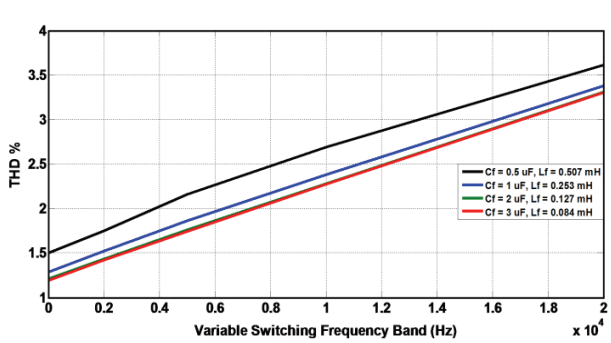

Fig. 12. Simulated THD% levels of load currents for different switching frequency bands through LLCL filters of the same tuning at 10 kHz.

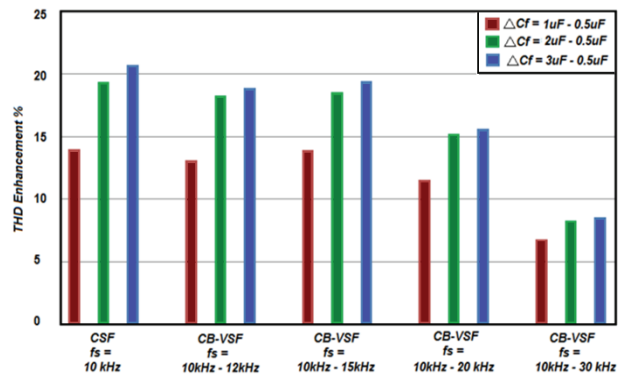

Fig. 13. Simulation results of the THD enhancement percentages using (20) with respect to the filter capacitor changing.

discussion on the selection of the LLCL filter parameters, particularly on the tuning branch capacitance C_f.

While a larger C_f is preferred in terms of THD performance, the selection of C_f using (14) was proven to be effective since it allows for the use of a smaller C_f (less reactive power absorbed), while providing comparable THD performance with a larger C_f value.

VI. Experiment Results

To validate the simulation results, an experimental rig including a full bridge single phase inverter and an LLCL filter has been implemented based on the parameters listed in Table I and Table II using a Texas Instruments TMS 320F28335 digital signal processor (DSP) board. The 10 kHz CSF PWM and CB-VSF PWM schemes were then implemented using different VSF bands (2 kHz, 5 kHz, 10 kHz and 20 kHz) and four LLCL filters with different L_f and C_f components (all of them were selected with the same 10 kHz tuning frequency).

The method in [18] was adopted to implement the CB-VSF PWM technique based on the unipolar strategy. The experimental work was carried out in an open-loop manner without a current controller. Since the main focus of this paper is to propose the design guidelines of an LLCL filter for variable switching frequency PWM, a current controller was not included in this paper. Due to page limitations, the design of the current controller and is performance will be included in a future work.

Fig. 14 shows PWM pulses generated by the DSP unit based on the CB-VSF PWM technique with a 5-10 kHz frequency (5 kHz band).

Due to the unipolar switching strategy, the actual switching harmonics appear from 10-20 kHz i.e. with a 10 kHz band. From Fig. 14, it is noticeable that CB-VSF PWM has a regular frequency variation. Figs 15 and 16 show the experimental harmonic spectrum and THD levels of the load side currents (after the LLCL filter) using 10 kHz CSF PWM.

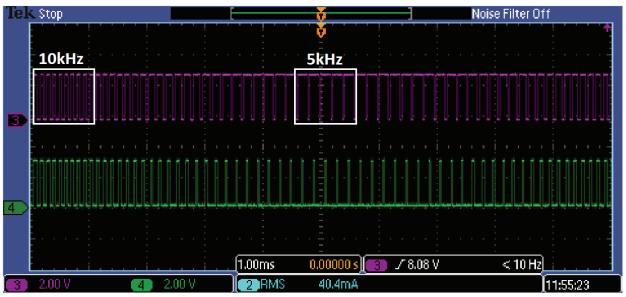

Fig. 14. PWM pulses of CB-VSF PWM for band (5-10 kHz), pulses of S1, S2' (CH3) and S3, S4' (CH4).

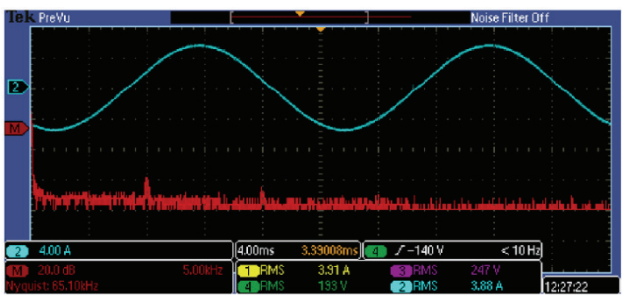

(a)

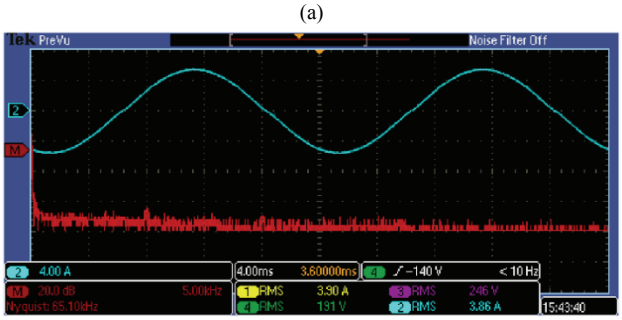

(b)

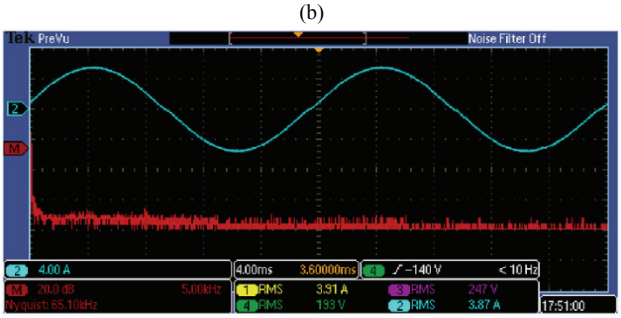

(c)

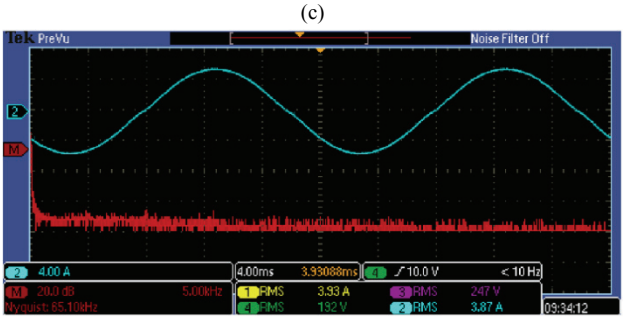

(d)

Fig. 15. Experimental load current (blue) with its spectrum (red) at 10 kHz CSF PWM using *LLCL* filters of the same f_s tuning: (a) $C_f = 0.5$ μF, $L_f = 0.507$ mH; (b) $C_f = 1$ μF, $L_f = 0.253$ mH; (c) $C_f = 2$ μF, $L_f = 0.127$ mH; (d) $C_f = 3$ μF, $L_f = 0.084$ mH.

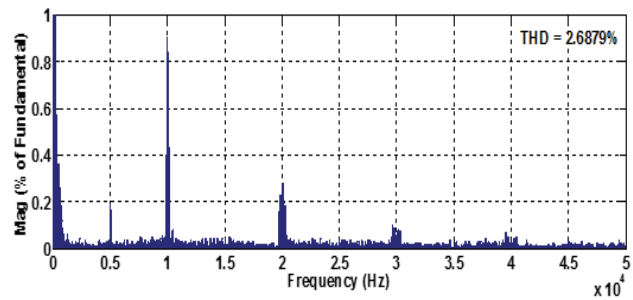

(a)

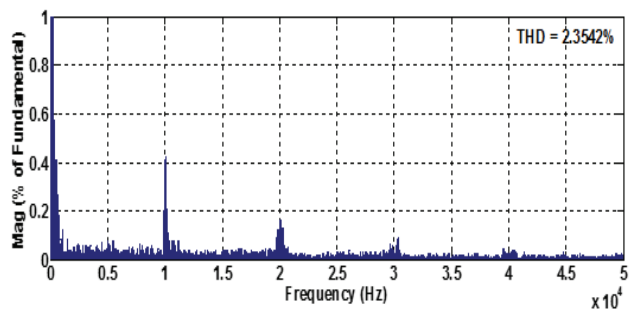

(b)

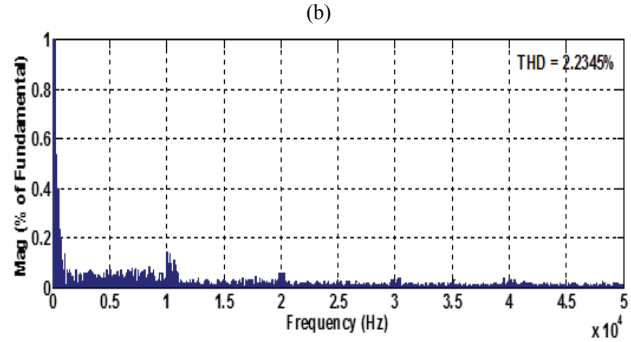

(c)

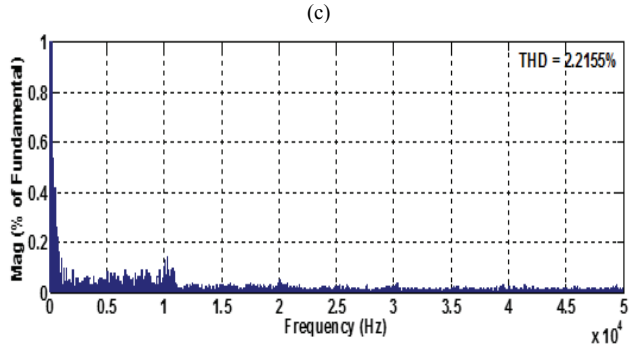

(d)

Fig. 16. Experimental harmonic spectrums of load current based on 10 kHz CSF PWM using *LLCL* filters of the same f_s tuning: (a) $C_f = 0.5$ μF, $L_f = 0.507$ mH; (b) $C_f = 1$ μF, $L_f = 0.253$ mH; (c) $C_f = 2$ μF, $L_f = 0.127$ mH; (d) $C_f = 3$ μF, $L_f = 0.084$ mH.

The effect of increasing the filter capacitor on reducing the harmonic spectrum is markedly noticeable. As seen in the simulation, while increasing C_f helps to reduce the THD, further increasing of C_f from 2 μF to 3 μF does not provide a significant improvement in the THD. Similar observations can be made for 10-20 kHz CB-VSF PWM (10 kHz band), as seen in Fig. 17 and Fig. 18.

Table IV shows the THD percentage levels of the load

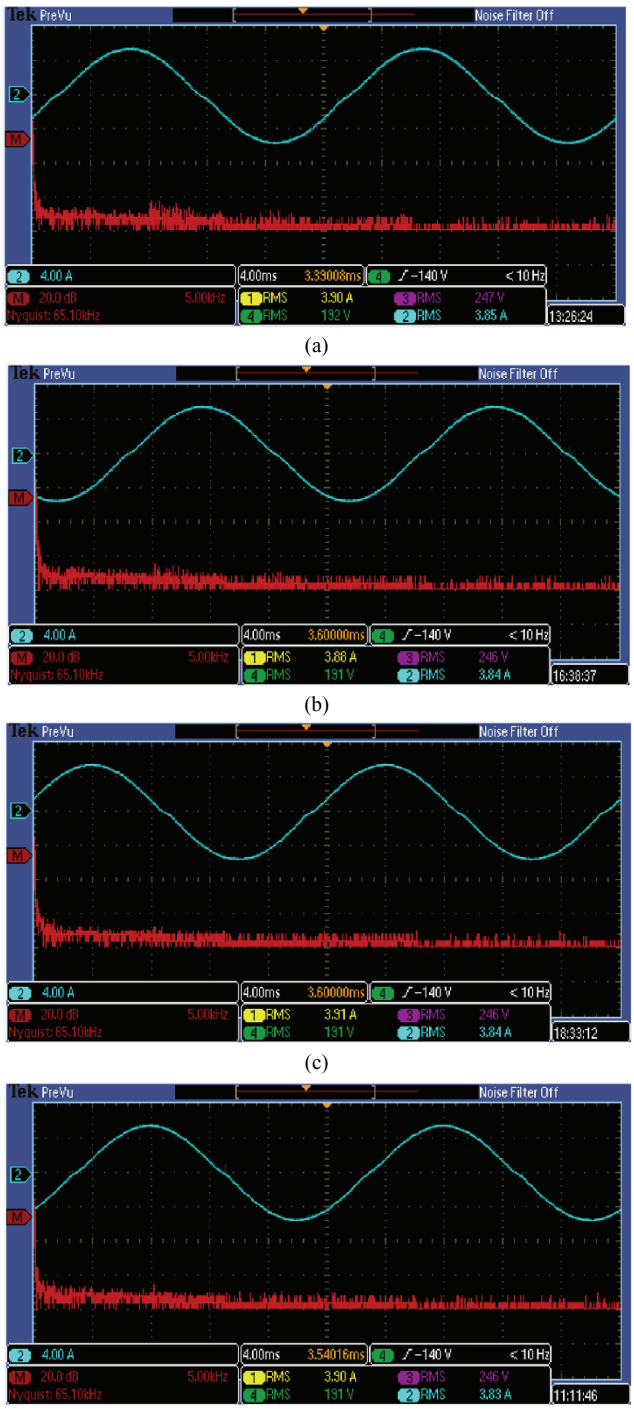

Fig. 17. Experimental load current (blue) with its spectrum (red) at 10-20 kHz CB-VSF PWM using LLCL filters of the same tuning at f_{VSFmin}: (a) C_f = 0.5 μF, L_f = 0.507 mH; (b) C_f =1 μF, L_f = 0.253 mH; (c) C_f = **2** μF, L_f = 0.127 mH; (d) C_f = 3 μF, L_f = 0.084 mH.

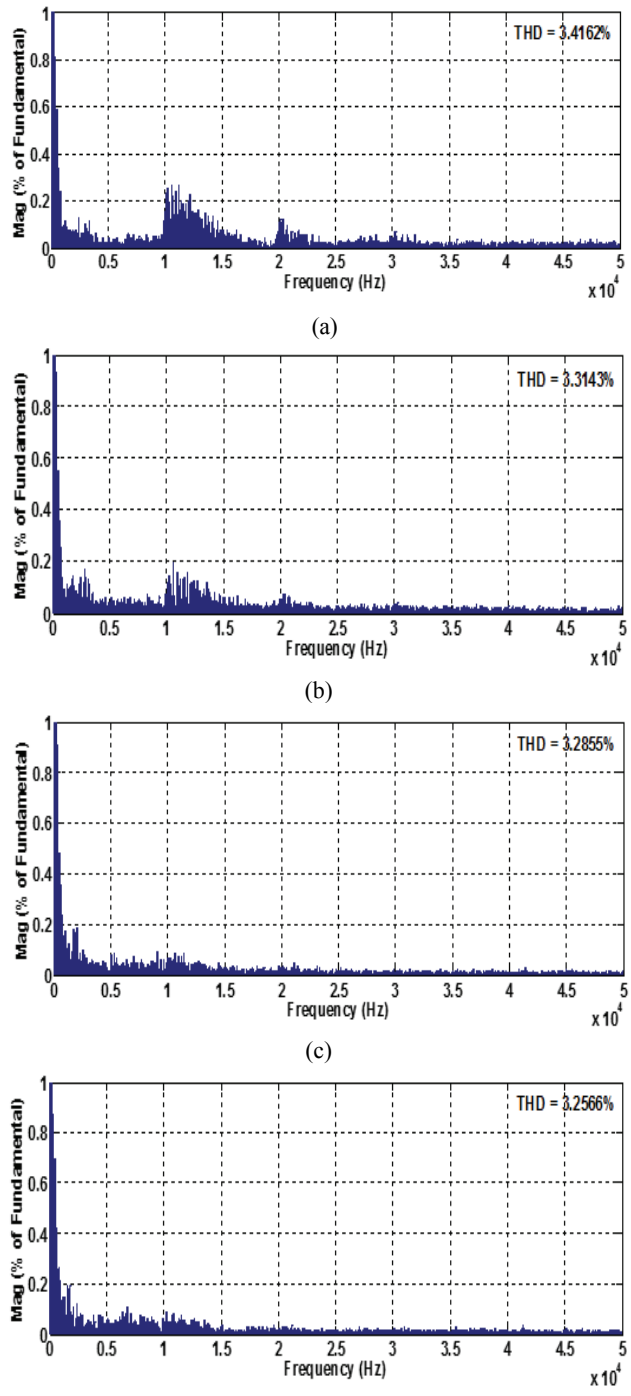

Fig. 18. Experimental harmonic spectrums of load current at 10-20 kHz CB-VSF PWM using LLCL filters of the same tuning at f_{VSFmin}: (a) C_f = 0.5 μF, L_f = 0.507 mH; (b) C_f = 1 μF, L_f = 0.253 mH; (c) C_f = 2 μF, L_f = 0.127 mH; (d) C_f = 3 μF, L_f = 0.084 mH.

currents for CSF PWM and CB-VSF PWM with different VSF bands, which are illustrated in Fig. 19.

The percentages of the THD improvements are calculated using (20) for all of the PWM methods in this study. These percentages are shown in Fig. 20, which confirms that increasing the filter capacitance is necessary to have better THD levels due to the lower equivalent impedance of the serial C_fL_f branch along the variable switching frequency band.

Due to the nonlinearity behavior of the filter capacitor

TABLE IV
EXPERIMENTAL THD PERCENTAGE LEVELS OF LOAD CURRENTS USING 10 KHZ TUNING AT DIFFERENT SWITCHING FREQUENCY BANDS

Switching Frequency	LLCL: 1 L_f = 0.507 mH C_f=0.5 μF	LLCL: 2 L_f= 0.253 mH C_f = 1 μF	LLCL: 3 L_f=0.127 mH C_f= 2 μF	LLCL:4 L_f=0.084 mH C_f= 3 μF
CSF PWM f_s = 10 kHz	2.6879	2.3542	2.2345	2.2155
CB-VSF PWM f_{VSF}=10-12 kHz	2.8561	2.6722	2.5637	2.5673
CB-VSF PWM f_{VSF}=10-15 kHz	3.0646	2.9179	2.8232	2.8432
CB-VSF PWM f_{VSF}=10-20 kHz	3.4162	3.3143	3.2855	3.2566
CB-VSF PWM f_{VSF}=10-30 kHz	3.9707	3.8548	3.8059	3.7885

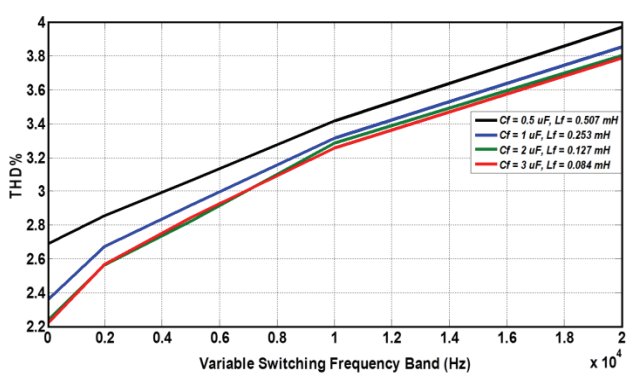

Fig. 19. Experimental load current THD% for different switching frequency bands.

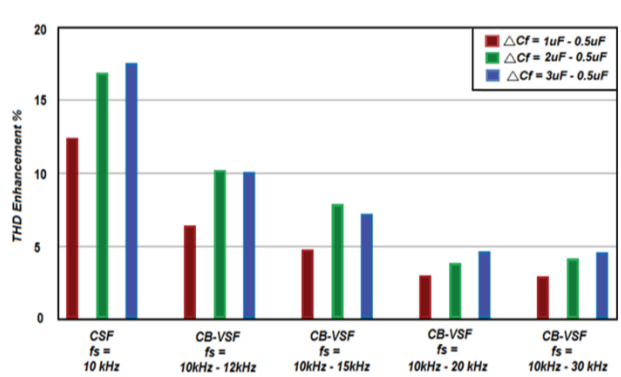

Fig. 20. Experimental THD enhancement percentages using (20) with respect to the filter capacitor changing.

impedance as explained in Section 3 (B), it is not necessary to select the maximum filter capacitor by which the system will absorb the maximum power limit.

The experimental results confirm the superiority of the 2 μF C_f over the 3 μF C_f for avoiding the 5% maximum limit of the absorbed reactive power.

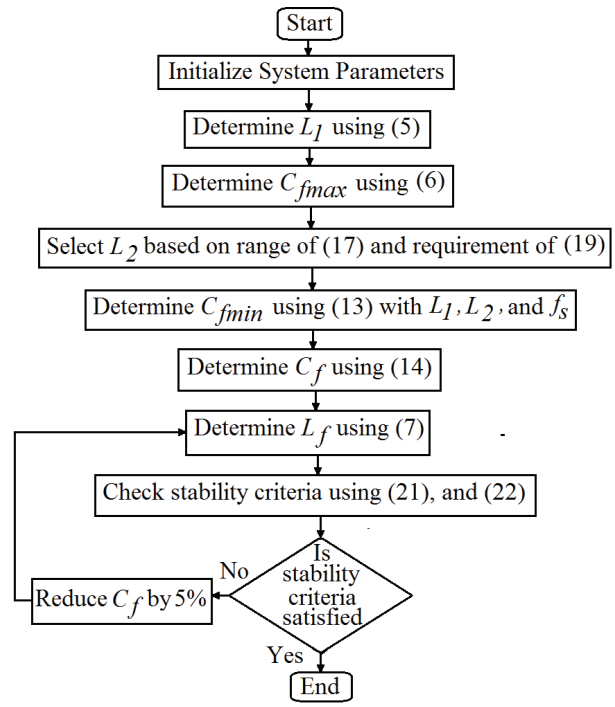

Fig. 21. Flowchart for selecting the LLCL filter components without a damping resistor for CBVSF PWM applications.

VII. LLCL FILTER PARAMETERS SELECTION PROCEDURE FOR CB-VSF PWM

Throughout the theoretical analysis as well as the simulation and experimental results, it is found that choosing LLCL filter parameters for CB-VSF PWM can be facilitated using the steps of the flowchart in Fig. 21. The general selection procedure is provided based on the discussion presented in Section 3, with an additional step for ensuring system stability.

It is known that LCL and LLCL filters have stability issues, which can be mitigated using a damping resistor in the tuning branch. However, this causes the filter performance to degrade. In addition, the optimal sizing of the damping resistor has been a topic of previous studies.

Recently, the authors of [10] found that the stability of an LLCL filter can be guaranteed without the use of a damping resistor if stability criteria (21) is satisfied:

$$f_s/6 \leq f_{rc} < f_r \tag{21}$$

$$f_{rc} = \frac{1}{2\pi\sqrt{(L_1 + L_f)\, C_f}} \tag{22}$$

This method is adopted here to ensure the robustness of the LLCL filter with grid operation.

The selection procedure starts with the initialization of the system parameters, i.e. the DC link voltage, grid voltage, system rated power, desired current ripple and minimum switching frequency. The inverter side inductor L_1 can be decided based on the desired value of the current ripple using (5). The maximum allowable value of the filter capacitor

C_{fmax} can be determined by considering 5% of the absorbed rated power using (6).

The grid side inductor L_2 can be selected in the range of (18), while considering that the selected L_2 value should be bigger than the minimum limit of the (18) or (19) range and agree with a grid condition 0.3% of the harmonics order > 35 [6]. After deciding and selecting L_2, the minimum limit of the filter capacitor C_{fmin} can be calculated using (13) by substituting the tuning frequency value at f_s and the value of the constant k from L_1 and L_2. Based on these facts, a lower LLCL filter attenuation is observed for high order harmonics at a low value of filter capacitor. Secondly, there is low enhancement in the filter attenuation and consequently in the THD of the load current between using the maximum filter capacitor C_{fmax} or a little lower C_{fmax}. This is done to avoid absorbing the maximum allowable 5% of the rated power and to avoid effecting the system stability. This paper proposes an average of the maximum and minimum filter capacitor limits ((C_{fmax}+ C_{fmin})/2) that is more reasonable in LLCL filter design for CBVSF PWM. The process of designing the components of the LLCL filter is shown in the flowchart of Fig. 21. The filter tuning branch inductor L_f can be determined using (7). After determining all of the LLCL filter parameters, the system stability status is checked based on the stability criterion in (21). If the criterion is not satisfied, the filter capacitor value should be reduced and a new value for the tuning inductor L_f should be determined. This process is repeated until the stability criterion is met.

VIII. CONCLUSIONS

A study of the design of an LLCL filter for the CB-VSF PWM technique is presented in this paper. The effects of the parameter selections for LLCL filters are discussed and compared in terms of harmonic spectrum and load current THDs. It can be concluded that the LLCL filter can be useful for CB-VSF PWM as long as different design considerations are taken. In addition, when placing the tuning frequency around the highest switching frequency harmonic, the filter needs to be designed to maximize the attenuation for the whole switching frequency band. By analyzing the effect of each parameter selection on the filter performance, it is found that increasing C_f improves the THD levels and the harmonics spectrum attenuation. However, this also increases the level of system reactive power absorption and effects negatively on the system stability, which makes it important to select a certain moderate capacitor value. Therefore, a general LLCL filter selection guideline is presented to allow for its use with the CB-VSF PWM method.

When compared to previous studies for LLCL filter parameter design, this study has the advantages of facilitating the LLCL filter parameter design for CBVSF PWM. Meanwhile, previous studies are only proposed for CSF PWM based inverter applications. In addition, the study analyzes the C_f and L_f changing effect on the harmonic attenuation effectiveness of the filter for the band of frequencies. Finally, this study provides guidelines for filter parameter design. The disadvantage of this proposal is the need for increasing C_f more than C_{fmin}, which increases the system reactive power absorption. This disadvantage was tackled by Eq. (14), which aims to select a moderate level of C_f to guarantee an acceptable level of reactive power absorption.

Simulation results and laboratorial investigations of a 1 kW single-phase inverter validated the theoretical discussion.

ACKNOWLEDGMENT

The authors would like to acknowledge the support provided by UM Power Energy Dedicated Advanced Centre (UMPEDAC), University of Malaya, Malaysia.

REFERENCES

[1] *Electromagnetic Compatibility (EMC)-Part 3: Limits-Section 6: Assessment of Emission Limits for Distorting Loads in MV and HV Power Systems*, IEC 1000–3–6, 1996.

[2] *IEEE Recommended Practices and Requirements for Harmonic Control in Electric Power Systems*, IEEE Std. 519-1992, 1992.

[3] M. Lindgren and J. Svensson, "Connecting fast switching voltage source converters to the grid – Harmonic distortion and its reduction," in *Proc. PTC, Stockholm*, pp. 191-195, 1995.

[4] P. Channegowda and V. John, "Filter optimization for grid interactive voltage source inverters," *IEEE Trans. Ind. Electron*., Vol. 57, No. 12, pp. 4106-4114, Dec. 2010.

[5] Y. Lang, D. Xu, S. R. Hadianamrei, and H. Ma, "A novel design method of LCL type utility interface for three-phase voltage source rectifier," *Power Electronics Specialists Conference, PESC '05. IEEE 36th*, pp. 313-317, 2005.

[6] W. Wu, Y. He, and F. Blaabjerg, "An LLCL power filter for single phase grid-tied inverter," *IEEE Trans. Power Electron*., Vol. 27, No. 2, pp. 782-789, Feb. 2012.

[7] J. Dannehl, F. W. Fuchs, and P. B. Thøgersen, "PI state space current control of grid-connected PWM converters with LCL filters," *IEEE Trans. Power Electron*., Vol. 25, No. 9, pp. 2320-2330, Sep. 2010.

[8] H.-G. Jeong, K.-B. Lee, S. Choi, and W. Choi, "Performance improvement of LCL-filter-based grid-connected inverters using PQR power transformation," *IEEE Trans. Power Electron*., Vol. 25, No. 5, pp. 1320-1330, May 2010.

[9] R. N. Beres, X.i Wang, M. Liserre, F. Blaabjerg, and C. L. Bak, "A review of passive power filters for three-phase grid connected voltage-source converters," IEEE J. Emerg. Sel. Topics Power Electron., Vol. 4, No. 1, pp. 54-69, Mar. 2016.

[10] M. Huang, X. Wang, P. C. Loh, and F. Blaabjerg, "LLCL-filtered grid converter with improved stability and robustness," *IEEE Trans. Power Electron*., Vol. 31, No. 5, pp. 3958-3967, May 2016.

[11] M. Huang, P. C. Loh, W. Wu, and F. Blaabjerg, "Stability analysis and active damping for LLCL-filter based grid-connected inverters," in *Proc. IPEC*, pp. 2610-2617, 2014.
[12] M. Huang, W. Wu, Y. Yang, and F. Blaabjerg, "Step by step design of a high order power filter for three-phase three-wire grid-connected inverter in renewable energy system," in *Proc. PEDG*, pp. 1-8, 2013.
[13] K. Dai, K. Duan, X. Wang, and Y. Kang, "Application of an LLCL filter on three-phase three-wire shunt active power filter," in *Proc. IEEE INTELEC*, pp. 1-5, Sep. 2012.
[14] W.-Y. Sung, H. M. Ahn, J.-H. Ahn, and B. K. Lee, "Sensorless active damping method for an LCL filter in grid-connected parallel inverters for battery energy storage systems," J. EET, Vol. 13, No. 1, pp. 280-286, Jan. 2018.
[15] H. M. Ahn, C.-Y. Oh, W.-Y. Sung, J.-H. Ahn, and B. K. Lee, "Analysis and design of LCL filter with passive damping circuits for three-phase grid-connected inverters," *J. Electr. Eng. Technol*., Vol. 12, No. 1, pp. 217-224, Jan. 2017.
[16] R. L. Kirlin, C. Lascu, and A. M. Trzynadlowski, "Shaping the noise spectrum in power electronic converters," *IEEE Trans. Ind. Electron*., Vol. 58, No. 7, pp. 2780-2788, Jul. 2011.
[17] X. Mao, R. Ayyanar, and H. K. Krishnamurthy, "Optimal variable switching frequency scheme for reducing switching loss in single-phase inverters based on time-domain ripple analysis," *IEEE Trans. Power Electron*., Vol. 24, No. 4, pp. 991-1001, Apr. 2009.
[18] H. A. Attia, T. K. S. Freddy, H. S. Che, W. P. Hew, A. El Khateb, "Confined band variable switching frequency pulse width modulation (CB-VSF PWM) for single-phase inverter with LCL filter," *IEEE Trans. Power Electron*., Vol. 32, No. 11, pp. 8593-8605, Nov. 2017.
[19] J. K. Phipps, "A transfer function approach to harmonic filter design," *IEEE Ind. Appl. Mag*., Vol. 3, No. 2, pp. 68-82, Mar./Apr. 1997.
[20] D. G. Holmes and T. A. Lipo, *Pulse Width Modulation for Power Converters*, New York: Wiley, 2003.
[21] Insulated Gate Bipolar Transistor With Ultrafast Soft Recovery Diode IGBT: IRG4PH50KDPbF Datasheet, 2004. [Online]. Available: http://www.irf.com.

Hussain A. Attia was born in Baghdad, Iraq, in 1969. He received his B.S. and M.S. degrees in Electronic Engineering from the University of Technology, Baghdad, Iraq, in 1991 and 1999, respectively. He is presently working towards his Ph.D. degree at the University of Malaya, Kuala Lumpur, Malaysia. Since 2000, he has been working on many research projects in power electronics and renewable energy generation as well as their application fields (design and implementation) such as (1ph and 3ph) PWM inverters, robot car park (PLC control), PV electric vehicles, fuel cell electric vehicles, and decentralized street LED light dimming systems. In addition, he has published many papers on various research projects. He served as a technical and organizing member for many IEEE and international conferences such as ICEDSA / 2016, ICECTA / 2017 and ICEWES / 2018. His current research interests include harmonic reduction techniques, PWM techniques, inverters/ converters for renewable energy systems, AC/DC drives and digital design.

Tan Kheng Suan Freddy received his BEng degree in Electrical Engineering from the Multimedia University, Malaysia, in 2010; and his Ph.D. degree from the University of Malaya, Kuala Lumpur, Malaysia, in 2015. He is presently serving as a Lecturer in the Asia Pacific University of Technology and Innovation (APU), Kuala Lumpur, Malaysia. Prior to working at APU, he was a Postdoctoral Research Fellow in the UM Power Energy Dedicated Advanced Centre (UMPEDAC), University of Malaya. Dr. Freddy was a recipient of an ASEAN-Korea Exchange Fellowship Award. He was a Visiting Research Scholar in the Power Electronics Laboratory, Ajou University, South Korea. His current research interests include power electronics converters, renewable energy and smart grids.

Hang Seng Che received his B.Eng. degree in Electrical Engineering from the University of Malaya, Kuala Lumpur, Malaysia, in 2009; and his Ph.D. degree in Electrical Engineering under the auspices of a dual Ph.D. program between the University of Malaya and Liverpool John Moores University, Liverpool, ENG, UK, in 2013. Since 2013, he has been with UM Power Energy Dedicated Advanced Centre (UMPEDAC), University of Malaya, where he is presently serving as a Senior Lecturer. Dr. Che has been an Associate Editor of the IET Electric Power Applications Journal since 2016. He received a 2009 Kuok Foundation Postgraduate Scholarship Award for his Ph.D. studies, and a Frontier Researcher Award in 2016 from the Malaysian Ministry of Higher Education for his research work. His current research interests include multiphase machines and drives, fault-tolerant control, and power electronics converters for renewable energy applications.

Ahmad H. El Khateb received his B.S. and M.S. degrees from the Islamic University of Gaza, Gaza City, Palestine, in 2005 and 2007, respectively; and his Ph.D. degree in Power Electronics from University of Malaya, Kuala Lumpur, Malaysia, in 2013. He is presently working as a Lecturer in Power Electronics with the School of Electronics, Electrical Engineering and Computer Science (EEECS) at the Queen's University Belfast, Belfast, NI, UK. He has been working in the areas of power electronics, renewable energy generation, and grid integration for over ten years and has made significant contributions to the industrial and power electronics research community in the form of literature and prototype research platforms. He is an IEEE Senior Member. He also coordinated the IET Megaw Memorial Lecture in 2018, and was the local organizing Chair for the Irish Signals and Systems Conference (ISSC 2018), held in Belfast, NI, UK, in June 2018.